Sustainable Energy Technologies and Assessments 31 (2019) 262–272

Contents lists available at ScienceDirect

Sustainable Energy Technologies and Assessments

journal homepage: www.elsevier.com/locate/seta

Comparative study of the influence of a wave energy converter site on the wave field of Laguna, SC, Brazil

Phelype Haron Oleinik[a,*], Thaísa Beloti Trombetta[a], Ricardo Cardoso Guimarães[a], Eduardo de Paula Kirinus[a], Wiliam Correa Marques[b]

[a] Escola de Engenharia, Universidade Federal do Rio Grande, Campus Carreiros, Av. Itália s/n Km 8, CEP 96201-900, Brazil
[b] Instituto de Matemática Estatística e Física, Universidade Federal do Rio Grande, Campus Carreiros, Av. Itália s/n Km 8, CEP 96201-900, Brazil

ARTICLE INFO

Keywords:
Wave energy
Sustainable energy
Wave model
Tomawac
OWC

ABSTRACT

Recently mankind has started to acknowledge the effects of climate change caused by the emission of pollutants to the atmosphere. This issue, combined with the increasing global energy demand, and the diminishing supply of the main energy sources, brings forward the urgency of novel sources renewable energy. The ocean waves are a relatively novel source of energy that could be exploited if correctly studied and developed, aiming to minimize the environmental impact and increase the power takeoff. Hence the object of this study is to estimate the wave energy reduction caused by the presence of wave energy conversion devices near the coastline of Laguna, Brazil. In order to study the coastal impact of a wave energy converter (WEC) farm, the third generation sea state model Tomawac, from the Open Telemac-Mascaret suite of free surface models, was used to simulate the waves on the Southern Brazilian Shelf under two different conditions, with and without the presence of an array of WECs. The results show that the mean Significant Wave Height in the blockaded area undergo a slight drop, caused by the presence of the WECs, that do not appear in the scenario without the devices.

Introduction

The global energy demand grows by the day with the technological advances, the industry expansion and the growth of the progressive urbanization of the world. This demand is rapidly depleting the current supplies and energy sources that the civilization is built upon, many of which consist of unsustainable sources, that are either non-renewable, or are harmful to the environment and the people.

Recent studies have focused on bringing forward novel ways to generate energy, and some have investigated the aspects of the electricity generation from sea waves. The study of wave energy generation is split into two major branches. One, on the engineering aspect of the study, is the design and development of the wave energy conversion devices (WEC) to attain the optimal geometry in order to get the best input-to-output ratio of conversion. The other, on the oceanographic aspect of the study, is the sea state simulation to determine the theoretical wave power available for conversion.

The study of the WEC devices is in an advanced stage of development. Drew et al. [1] evaluated the device types that represent current WEC technology, focusing on works within the United Kingdom, and considered strategies to enhance the efficiency of point absorber-type WECs. Falcão [2] described the development of wave energy utilization since the 1970s, focusing the characterization of the wave energy resources and the various technologies for WECs classified as Oscillating Water Column, Oscillating Bodies and Overtopping.

In order to study the performance of the converters, Babarit et al. [3] estimated the mean annual power absorption of a selection of eight WECs with different working principles, using computational modeling. López et al. [4] also described the physical principles involved in the conversion process as well as the infrastructure to implement WECs.

There are also studies focused on the challenges encountered for the installation of WECs in the ocean, as in the case of Tiron et al. [5], who commented on extreme events in the ocean, accessibility issues for maintenance, as well as environmental issues. In addition to that, Day et al. [6] reviewed key issues in the physical and numerical modeling of marine renewable energy systems, including wave energy devices, current turbines, and offshore wind turbines.

Amiri et al. [7] performed numerical simulations to improve the efficiency of floating point absorber converters, where the effects of wave potential on energy conversion were investigated. The results of this study may be used to improve the efficiency of this type of converter in certain circumstances, such as stations with low wave energy

* Corresponding author.
E-mail address: phe.h.o1@gmail.com (P.H. Oleinik).

https://doi.org/10.1016/j.seta.2018.12.023
Received 11 April 2018; Received in revised form 12 December 2018; Accepted 14 December 2018
2213-1388/ © 2018 Elsevier Ltd. All rights reserved.

potential. Wang et al. [8] summarized the principles of harvesting ocean energy by wave energy converters, and reviewed the prototypes and commercial devices deployed in the sea along one year.

In addition, the works by Titah-Benbouzid and Benbouzid [9], Ozkop and Altas [10], Mustapa et al. [11] and Rusu and Onea [12] bring an up-to-date description of technologies, equipments, usage and performance. Studies such as these provide the development and enhancement of new technologies in the field of wave energy converters, exploring systems that are still considered to be costly to implement and difficult to maintain. However, there are still several other areas which are poorly explored, especially when attempts are made to join oceanic simulations with WEC simulations.

Research in wave energy sources performing trials for each type of WEC device present a great advantage, providing an accurate value of converted wave energy or assessment locations. The computational cost of long simulation implies the consideration of one device at a time. In this sense, the major disadvantage of this method is that the only interaction taken into account is the wave action on the device, and not the other way around. Thus it is not possible to predict the impacts of these devices on the environment they are inserted.

On the other hand is the analysis of the sea state to determine the theoretical energy potential of the wind waves. One of the first studies of wave energy potential is that of Kinsman [13], who estimated the global wave energy potential using a mean wave height and period for the surface and integrated this along the overall length of the global coastlines.

Since then, better estimates have been made, with more sophisticated methods, most of them using either satellite [14] or model data [15], also integrating the net wave power resource along the coastline. A more accurate estimate was performed by Reguero et al. [16], that have taken into account the direction from which the waves are coming. And one of the latest estimates, by Reguero et al. [17], was made using an “effective length” approach that considers only the coastline length perpendicular to the waves’ energy flux.

All of these are undeniably good estimates, all of them using robust methods and validated datasets. But the only problem is that they are the theoretical wave energy potential. They hardly represent the real amount of converted wave energy.

The main goal of this work is to join the wave energy resource assessment with the wave energy conversion process to answer how much does a wave farm can actually convert. This study uses a third generation wave model to simulate the sea state and, coupled to it, a newly developed wave energy conversion model that will interact with the wave model and return the amount of energy converted, as well as the influence of the WEC device on the wave field and the repercussion of this on the nearby coastline.

The study area

The study area was chosen based on the works of Oleinik et al. [18–20] who have pointed that, from the South and Southeastern Brazilian Shelf, the most energetic spots are at the coastal regions of Laguna, SC, of Ilhabela, SP, and of Farol Island, RJ. These authors pointed that the most energetic of the three locations is the Farol Island, but it is also subject to the greatest temporal variability.

Winds tends to prevail in the NE direction, delivering a monotonic south current, but in terms of seasonal variability [21], synoptic wind stress can promote or reverse the along-shelf flow transport for both the winter and summer seasons [22]. The atmospheric circulation of the Southern Brazilian Shelf varies, being directly influenced by the South Atlantic Subtropical Anticyclone (SASA), in addition to a propagation zone for low-pressure systems that usually carry cold fronts [23].

The SASA is responsible for good thermodynamic stability, resulting in NE winds of weak intensity. During summer, the SASA becomes weaker (at 32° S) and is farther from the coast, while during winter, the core is located northward at 27° S and loses its ability to maintain steady NE winds [23]. In addition, during winter, transient cold frontal systems arrive from the SBS. These systems enhance wind gusts, establishing the South Atlantic convergence zone from November to March [24] and increasing the frequency of frontal systems to one per week [23]. During summer, this number decreases, and it increases again in the spring [25].

The importance of better understanding atmospheric dynamics and its variability is related to the wave generation process and how it varies each season [17,20]. According to Espindola and Araújo [26], the wave direction presents a clear distinction from low latitudes to high latitudes. These waves can be harvested for energy conversion despite a relatively low power level because they present a high seasonal stability north of 28° S [27]. For the present paper, the location chosen is the coastal region of the Cape of Santa Marta, in the city of Laguna, in Santa Catarina state, despite being the less energetic, is the one with higher stability of wave resources.

The region nearby Cape of Santa Marta presents significant wave heights ranging from 1.5 m to 2.5 m, with wave period around 8 s to 10 s. These estimations of sea state are corroborated by Espindola and Araújo [26] and Oleinik et al. [20].

Fig. 1 shows the computational grid used for the simulation, which extends from Mostardas, RS on the south to Itanhaém, SP on the north. At the center of the coastline comprised by the computational domain, is the Cape of Santa Marta. The computational grid extends itself approximately 700 km towards the ocean, to the depth of 4000 m. The distance between the mesh nodes is approximately 10,000 m in deep ocean, reducing to 500 m on the coastal area, and 100 m at the study area.

The time period used for the case study is the year of 2014 because, in average, the El Niño index is nearly zero,[1] thus it does not have a significant influence on the results.

Section ‘Material and methods’ of this paper will briefly describe the wave model used, a brief description of the conversion model and the coupling scheme with Tomawac; Section ‘Results’ will present the case study and the results; and Section ‘Conclusion’ will contain a brief discussion of the results and conclude the paper with a few remarks of the possible consequences of such wave farm installed near the coastline.

Material and methods

The wave model—Tomawac

The wave model used on this study is the third generation sea state model Tomawac (Telemac-Based Operational Model Addressing Wave Action Computation), part of the Open Telemac-Mascaret modeling suite. Tomawac solves the Eq. 1 of conservation of wave action density for the directional wave spectrum:

$$\frac{\partial N}{\partial t} + \frac{\partial(\dot{x}N)}{\partial x} + \frac{\partial(\dot{y}N)}{\partial y} + \frac{\partial(\dot{k}_x N)}{\partial k_x} + \frac{\partial(\dot{k}_y N)}{\partial k_y} = Q(k_x, k_y, x, y, t) \quad (1)$$

where N is the directional wave spectrum, x and y are the orthogonal directions of the coordinate system, k_x and k_y are, respectively, the components in x and y of the wave number vector, and t is the time. Eq. 1 represents that, in a general situation of waves propagating in a non-homogeneous and unsteady environment, the wave action density is preserved within the source and sink terms, defined by Q [28].

Tomawac solves the propagation of the wind-driven waves and takes into account their gain and loss of energy by the main processes involved, such as the wind action, bottom friction-induced dissipation, shoaling, whitecapping, depth-induced refraction, and the non-linear interactions between waves.

Tomawac represents the sea state by splitting the directional wave

[1] www.esrl.noaa.gov/psd/enso/mei.

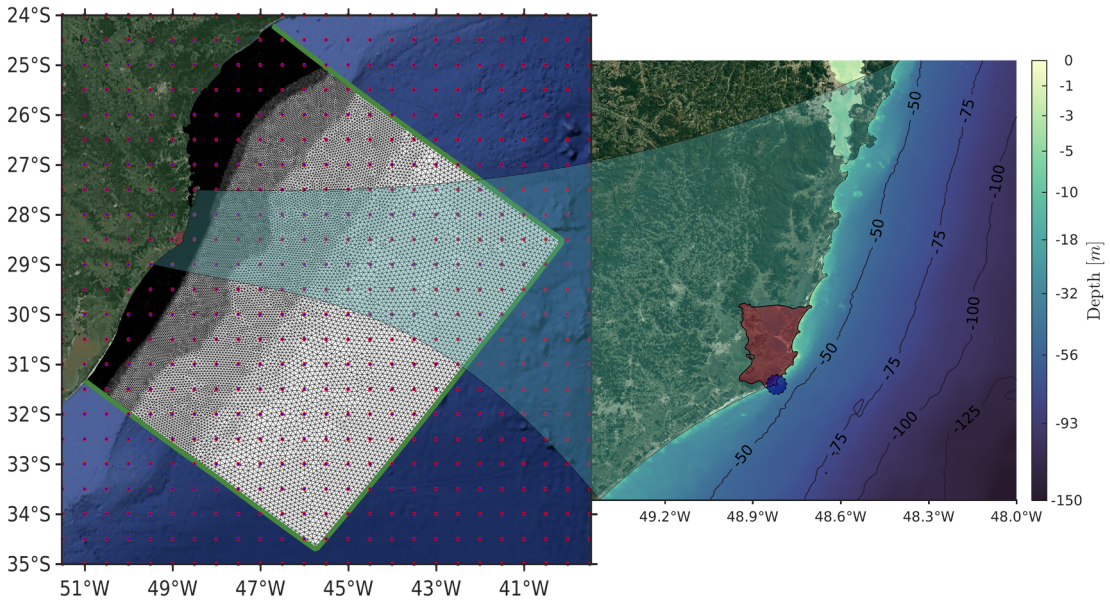

Fig. 1. Representation of the computational grid along the Brazilian coastline. The green lines around the mesh in the figure to the left show where the boundary conditions are imposed, and the gridded dots show the grid of the dataset used to generate the boundary conditions and the wind field. The figure to the right shows a detail of the coastline with the city of Laguna highlighted, and the circle shows the Cape of Santa Marta.

spectrum into a finite number of frequencies and directions ($N(f, \theta)$), then solves Eq. (1) for each component (f_i, θ_i) of the spectrum using the finite element method.

The integration of the wave energy spectrum ($E(f, \theta)$) along the discretized frequencies and directions gives the energy per unit area of the multi directional random wave field:

$$\sum_{f}^{f+df} \sum_{\theta}^{\theta+d\theta} \frac{1}{2}\rho g a_m^2 = E\left(f, \theta\right) df d\theta \tag{2}$$

where ρ is the specific mass of the medium, g is the acceleration of gravity, and a_m is the amplitude of each wave component. The wave energy spectrum (E) relates to the directional spectrum (N) by Eq. (3), where σ is the angular frequency of the waves:

$$E(f, \theta) = N(f, \theta)\rho g \sigma \tag{3}$$

The wave energy conversion model

In usual circumstances sea wave periods are up to 30 s, which representation requires a minimum sampling rate of 15 s, making the time domain representation of sea surface data infeasible for large scale applications. But for small scale processes, such as wave energy conversion device modeling, the time domain representation is more useful because it allows the representation of short scale processes, which prevail in these situations.

In order to couple the large-scale modeling of the sea state with the short-scale processes of the WEC device, this paper proposes a simplified approach to simulate the behavior of an Oscillating Water Column (OWC) device subject to a time series of sea surface elevation (η) which is obtained from the sea state spectrum simulated by Tomawac.

The Fourier Transform of a real-valued variable (such as the sea surface elevation) is a complex-valued function, whose real and imaginary parts compose the spectrum of said variable. This operation yields the amplitude spectrum of the sea surface, while the phase data is discarded following the assumption that it is randomly distributed in the interval $[0, 2\pi]$ [29].

To transform back the spectrum ($\mathscr{S}$) into a time series of sea surface elevation, one has to provide the IFT (Inverse Fourier Transform) the amplitude and phase spectra of the sea surface elevation. Since spectral wave models don't keep track of the wave phase, one can take advantage of the random distribution of this variable and supply the wave phase to the IFT as a randomly distributed variable in the interval $[0, 2\pi]$. With this, one can write the Fourier Transform of the sea surface elevation ($\mathscr{F}(\eta)$) as the combination of the amplitude data from the spectrum and the generated random phase data, then the sea surface elevation can be obtained by applying the IFT to the aforementioned $\mathscr{F}(\eta)$, obtaining η.

The resulting sea surface elevation time series, if long enough to eliminate statistical bias, will be equivalent to the original spectrum: their variance is the same; the spectral significant wave height and the significant wave height measured from the time series (using, for instance, the zero-up crossing method) are the same; and, mainly, the spectrum of η is identical to the original spectrum.

The wave energy conversion model developed for this paper was designed to use the raw directional spectrum from the spectral wave model (generalized here as "spectral wave model" because it can work in any spectral model with approximately the same characteristics) to simulate the energy conversion.

When coupled with Tomawac, the conversion module takes the wave spectrum at the specified mesh nodes and then applies an IDFT (Inverse Discrete Fourier Transform) algorithm to transform the spectral data into a time series of sea surface elevation, using the procedure described above.

To calculate the amount of converted energy the conversion module uses a simplified approach to represent an offshore OWC. This simplified approach is employed because a detailed simulation of an OWC would require a large computational effort, which would make infeasible a mid-term simulation such as the one in this paper.

The aforementioned simplification considers the OWC as a square semi-submerged chamber with its base open to the sea, and an aperture to the atmosphere where the turbine is located. The water-air interface inside the OWC chamber is assumed to be indeformable, and the air inside the chamber is approximated to be incompressible. Furthermore, the elevation of the surface inside the OWC is assumed to be forced only by the waves outside the chamber, so that the hypotheses of the linear wave theory hold true in this region.

That said, one can write the force balance between the inside and outside of the chamber:

$$\underbrace{\int_{-d}^{-l} \rho g\left(\zeta - z\right)\mathrm{d}z}_{\text{Internal hydrostatic force}} = \underbrace{\int_{-d}^{-l} \rho g\left(-z\right)\mathrm{d}z}_{\text{External hydrostatic force}} + \underbrace{\int_{-d}^{-l} \rho g\eta \frac{\cosh(k\,[d+z])}{\cosh(kd)}\mathrm{d}z}_{\text{Wave induced force}} \tag{4}$$

where d is the mean water depth, l is the submerged lip of the OWC, ρ is the specific mass of water, g is the gravity acceleration, k is the wave number, ζ is the elevation of the surface inside the OWC chamber measured from $z = 0$ and z is the vertical coordinate, positive upwards.

Integrating the equation the hydrostatic terms cancel out and Eq. (4) results in:

$$\rho g\zeta z|_{-d}^{-l} = \frac{\rho g\eta}{k}\frac{\sinh(k\,[d+z])}{\cosh(kd)}\Bigg|_{-d}^{-l} \tag{5}$$

which, substituting the limits and defining the height between the sea bottom and the OWC wall $h = d - l$ finally yields:

$$\zeta = \frac{\eta}{kh}\frac{\sinh(kh)}{\cosh(kd)} \tag{6}$$

which describes the surface inside the OWC in terms of the wave conditions outside.

With ζ one can then apply Betz [30]'s law to obtain the maximum available pneumatic power in the turbine of the OWC. This power is then subject to device-specific conversion processes and losses to then return the actual amount of converted energy. These device-specific information is not readily available since there is very few studies and prototypes that provide this, so they were not implemented in the conversion module, therefore the power obtained is the maximum available pneumatic power in the turbine. Fig. 2 shows a schematic of the conversion module and its coupling with TOMAWAC.

This attenuated sea surface height series is then subject to a Discrete Fourier Transform to convert it back into the spectral form, and then it

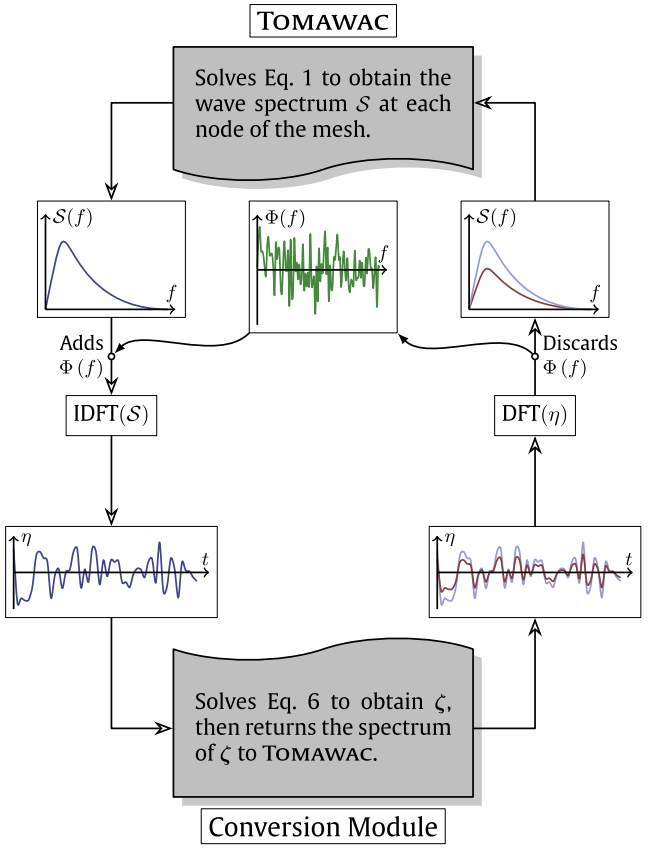

Fig. 2. Schematic of the conversion module coupled with TOMAWAC.

Table 1
Parametrization used for TOMAWAC for the case study simulation. Values omitted from the table use the default from TOMAWAC's implementation [28].

Simulation parameters	
PARALLEL PROCESSORS	12
Discretization	
TIME STEP	900
NUMBER OF TIME STEP	35040
NUMBER OF FREQUENCIES	25
MINIMAL FREQUENCY	0.033333
FREQUENTIAL RATIO	1.15225
NUMBER OF DIRECTIONS	24
Superficial conditions	
CONSIDERATION OF A WIND	Yes
STATIONARY WIND	No
WIND GENERATION COEFFICIENT	1.8
WATER DENSITY	1025
SHIFT GROWING CURVE DUE TO WIND	0.015
Boundary conditions	
LIMIT SPECTRUM MODIFIED BY USER	Yes
BOUNDARY ANGULAR DISTRIBUTION FUNCTION	2
BOUNDARY WEIGHTING FACTOR FOR ADF	0.95
Bottom conditions	
BOTTOM FRICTION DISSIPATION	1
DEPTH-INDUCED BREAKING DISSIPATION	3
Method settings	
LINEAR WAVE GROWTH	1
WIND GENERATION	1
NON-LINEAR TRANSFERS BETWEEN FREQUENCIES	1
WHITE CAPPING DISSIPATION	1

is returned to the wave model as a reduced version of the input spectrum.

The model was written in an external module for easy utilization within the wave model's source code. The conversion module is written in FORTRAN 95 because TOMAWAC is also written in this language and because of its performance for scientific applications. The Fast Fourier Transform and its inverse were externally used from the FFTW (Fastest Fourier Transform in the West) library [31].

The calibration and validation of TOMAWAC for this region has already been performed for earlier studies by Oleinik et al. [18–20], thus it was omitted from this paper. The parametrization used for the simulation is presented in Tab. 1.

Once finished the computational setup, the case study simulations were executed and their results analyzed. For the simulations, TOMAWAC was initialized from the rest at the first day of 2014. The oceanic boundaries of the computational domain were forced by wave data (Significant Wave Height – H_s, Peak Period – T_p, and Mean Direction – D_p) with temporal resolution of 3 h, and wind fields with temporal resolution of 6 h from NOAA's WAVEWATCH III Production Hindcast,[2] with spatial resolution of 0.5° (Fig. 1).

The wave farm

The setup for simulating the modified case (referred to as "modified", the scenario with the WECs) was, as previously stated, identical to the natural scenario, but with the conversion module coupled to TOMAWAC. The wave energy conversion farm simulated was composed of

[2] http://polar.ncep.noaa.gov/waves/hindcasts/prod-multi_1.php.

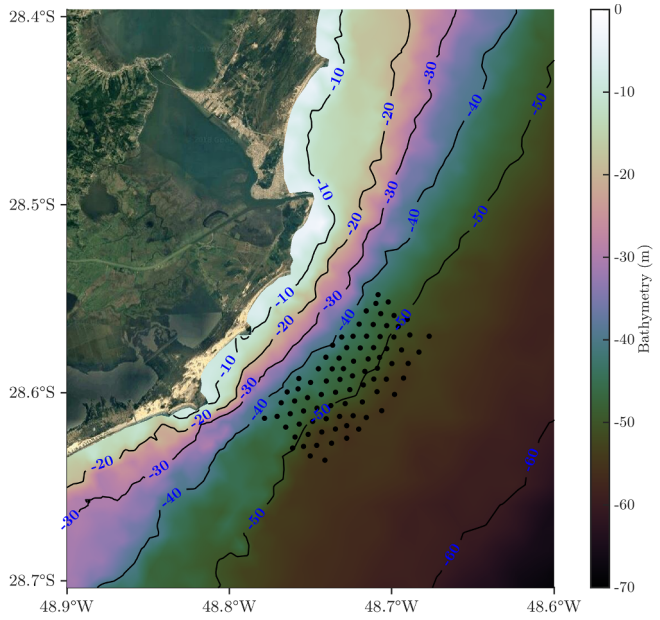

Fig. 3. Bathymetry of the coastal region around the Cape of Santa Marta and the location of the WECs simulated (black dots).

87 WECs distributed along a 10 × 5 km area, resulting in an arrangement where the distance between one WEC and another is approximately 800 m. This arrangement is shown in Fig. 3.

The extents of the wave farm, its location relative to the coastline, as well as the location of the WECs relative to each other was experimental, following some considerations: (1) Position the wave farm facing the main wave direction; (2) Follow the *aligned* configuration of López-Ruiz et al. [32]; (3) Maintain the distance between WECs up to 10 diameters, which according to Bozzi et al. [33] enhances the general farm power output.

The wave farm was chosen to be located around the location where the bathymetry is −50 m, because if the wave farm is too far off the coast, the maintenance costs are higher than expected, and if it is too close, the captured wave energy reduces too much.

The distance between each WEC was estimated to be enough for a small ship to navigate between them with a certain amount of security under favorable weather. From this the extents of the wave farm were derived.

Results

Two simulations were executed to provide the results for the present paper. The computational setup for both of them was exactly the same except for the fact that in one of them, the presence of the WEC devices was taken into account.

Global results

Firstly, since the results of both simulations in the offshore portion of the computational domain are identical, therefore only the global results of the natural case (referred to as "natural", the scenario without the WECs) will be presented.

Fig. 4a shows the time averaged Significant Wave Height (H_s) across the whole computational domain, ranging from 0.5 m in the Santos' Basin to 2.25 m on deep waters. This figure points toward the same conclusion presented by Oleinik et al. [18–20], who observed that in Laguna – SC, the average H_s of the waves was approximately 1.4 m. In addition, these authors showed that there is a remarkable increase in H_s in May and September, which are approximately the months that mark the transition between hot and cold weather.

For this study, it was observed that the mean of the waves in Laguna has the highest values in relation to the entire coast of Santa Catarina, reaching heights varying from 1.2 to 1.4 m near the coast.

Fig. 4b shows the time averaged Mean Period (T_m) in the computational domain, presenting values ranging from 6.75 s at the coastline, and slightly increasing towards the ocean up to 7.55 s. It is noticeable that in locations with higher H_s there is a higher value for T_m as well. It is worth noting that near the island of Florianópolis, there is a slight increase in the T_m, of approximately 0.25 s, which is an almost negligible value, that can be explained by either and actual increase in the period of the waves or by a reduction in the high-frequency part of the spectrum in that region.

It is also worth clarifying that due to the way the boundary conditions are imposed in Tomawac, the boundary nodes of the mesh and their immediate neighbors show some spurious figures for the output variables of the model, so they should be neglected.

Fig. 5a shows the time averaged Peak Period (T_p) over the computational domain. Its appearance is similar to the T_m (Fig. 4b), except that

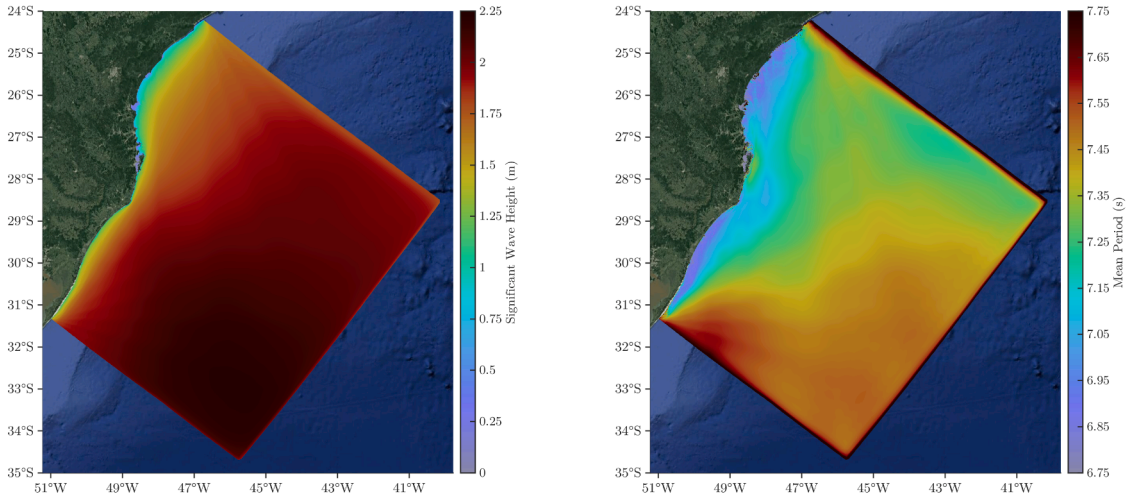

(a) Time averaged H_s. (b) Time averaged T_m.

Fig. 4. Time averaged H_s and T_m in the study area for the year of 2014.

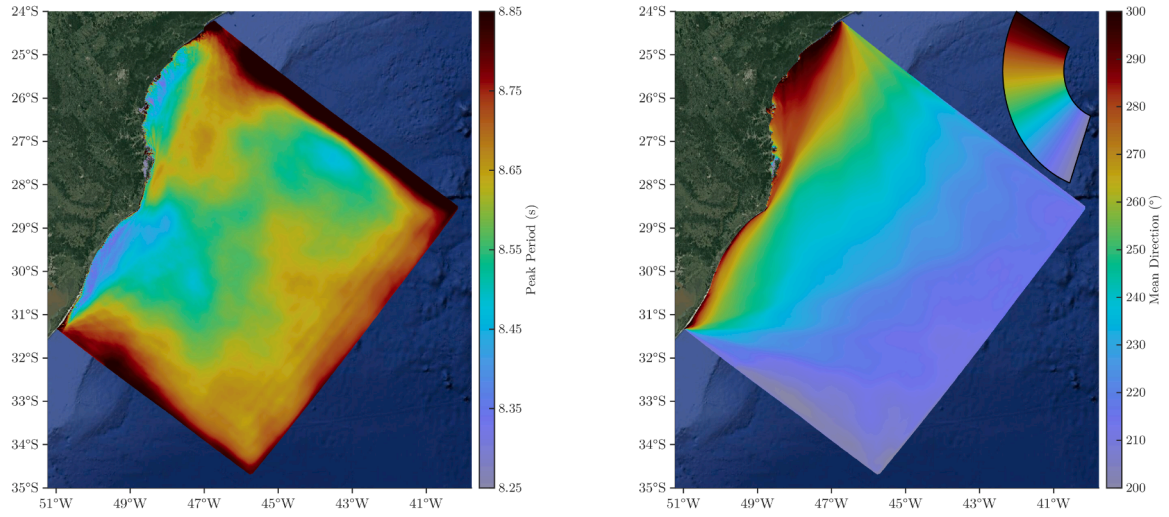

(a) Time averaged T_p. (b) Time averaged D_m.

Fig. 5. Time averaged T_p and D_m in the study area for the year of 2014.

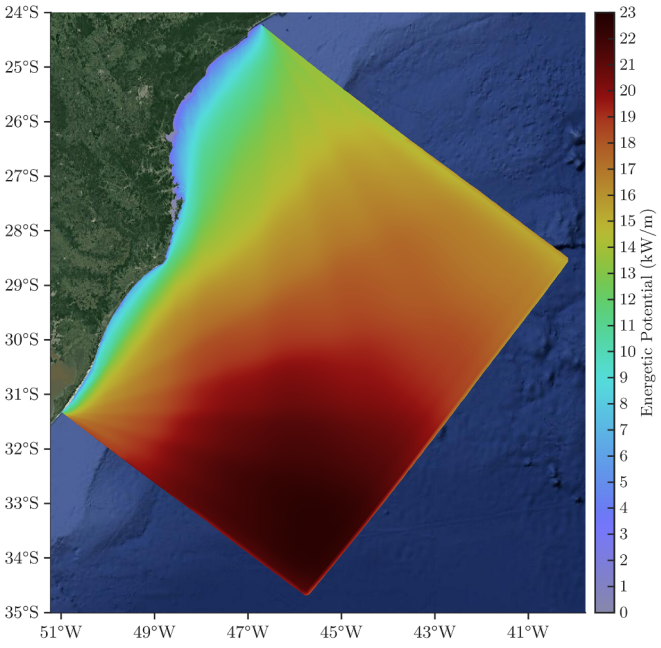

Fig. 6. Time averaged P_w in the study area for the year of 2014.

it is larger in value, but the general characteristics remain. Fig. 5b shows the mean travel direction (D_m) of the waves (the convention used is 0° for waves traveling towards the north and the positive values lie in the clockwise direction), and the disc section provides a visual representation of this direction.

Fig. 5b shows that the waves travel southwest in the ocean and deflect towards the coastline as they approach it, and near the coastline they are, in general, perpendicular to it.

Finally, Fig. 6 shows the mean Energetic Potential (P_w) in the computational domain, which has similar characteristics to those of H_s (Fig. 4a), with the smallest values in the Santos' Basin (less than 5 kW/m), and the largest ones close to the coastline at the Cape of Santa Marta, of approximately 12 kW/m. It is worth noting the contrast of the two mentioned regions; if one goes from the coastline at the Cape of Santa Marta towards the ocean, the values of P_w rapidly increase; otherwise, if one is at the Santos' Basin, the values of P_w increase much more slowly.

In accordance with this results, Guimarães et al. [34] showed that while at south region of Brazil, the values reach up to 11 kW/m near the coast, towards the north the values are from 5 to 8 kW/m. This greater difference of magnitude was explained by these authors due the incident direction of swell, which in the southern regions is predominantly south oriented.

Scenario comparison

The effect of the wave farm will be analyzed by means of the time averaged surfaces of the main wave parameters on the study area, and by means of the average difference of the two simulations.

The results of the modified scenario show, as one would expect, a reduction of the mean H_s (Fig. 7) of approximately 0.2 m (12%) at the position of the converters, but an unnoticeable reduction everywhere else.

This reduction is somewhat underestimated if compared to those of Abanades et al. [35], who found a reduction of approximately 50% on the point where the WEC is located. This discrepancy between the results is, most probably, related to the differences in the methods. Abanades et al. [35] used a WaveCat converter [36] instead of an OWC, and the conversion simulation was based on transmission coefficients [37].

The results of the T_m (Fig. 8) show, in average, an increase in the mean wave period on the location where the converters are installed, of approximately 0.25 s. This result, at first glance, seems incorrect but if one considers that T_m takes into account both the high and low frequency parts of the spectrum equally, when the waves are subject to a barrier, the high frequency part (*i.e.* the smaller waves) are quickly dissipated, while longer waves, although still affected, suffer less change from the action of the WECs. This leads to the high frequency (low period) part of the spectrum losing energy, raising the average.

The results of the T_p (Fig. 9), on the other hand, do not change significantly from one simulation to another, being increased by 0.05 s. But this result also makes sense, since the peak period is, by definition, the wave period where the wave spectrum has the most energy. To change this value significantly, the WEC would have to either partially remove this wave frequency from the spectrum, which does not happen because the OWC is a slender structure compared to the size of the

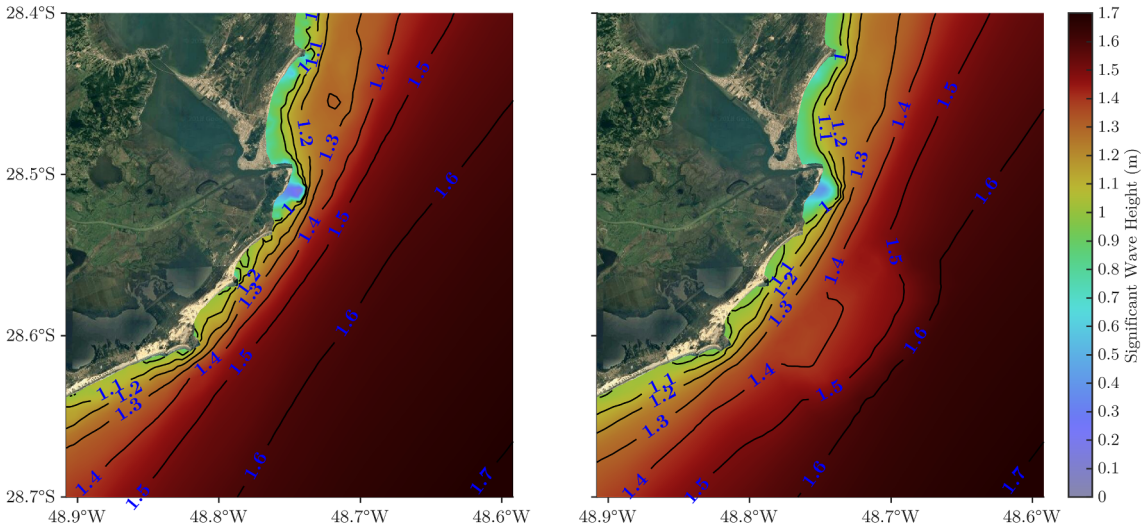

Fig. 7. Comparison of the time averaged H_s field for the (a – left) natural scenario and the (b – right) modified scenario.

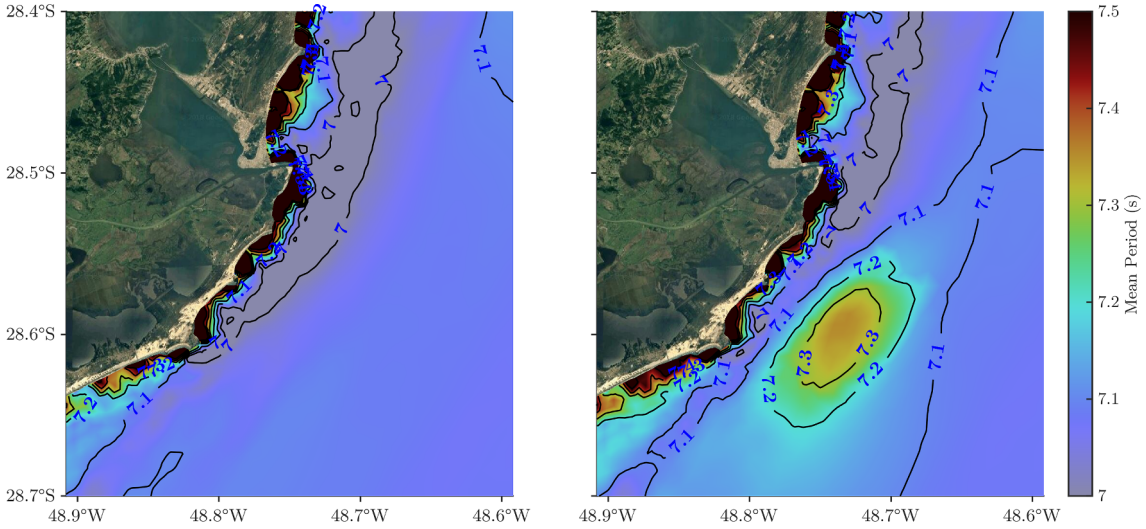

Fig. 8. Comparison of the time averaged T_m field for the (a – left) natural scenario and the (b – right) modified scenario.

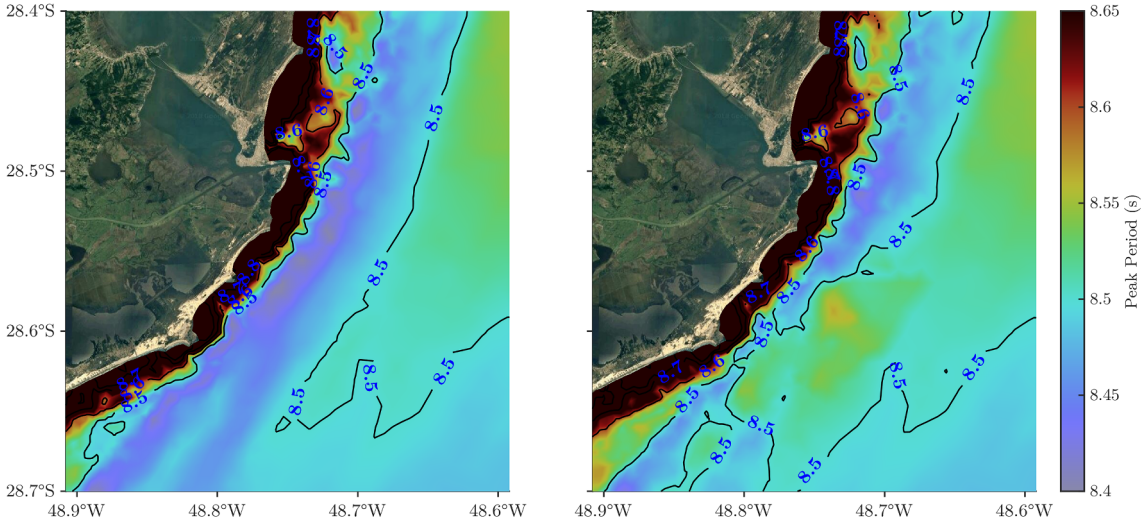

Fig. 9. Comparison of the time averaged T_p field for the (a – left) natural scenario and the (b – right) modified scenario.

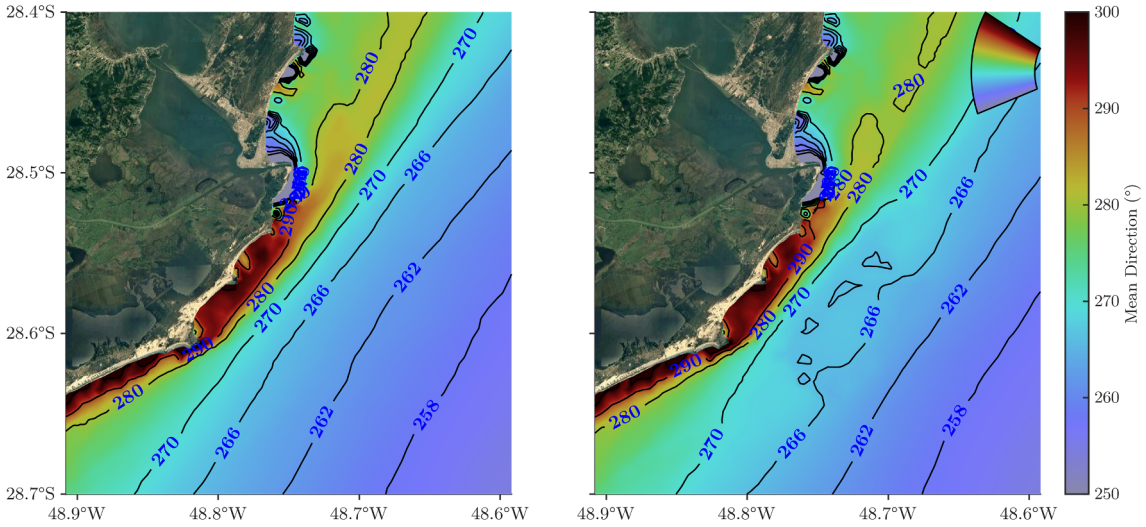

Fig. 10. Comparison of the time averaged D_m field for the (a – left) natural scenario and the (b – right) modified scenario.

waves; or it would have to drastically change the shape of the waves for them to have a different period, which is also not something a structure of this size can to easily.

An important result for this paper is the direction of the waves, which is one of the main factors controlling sediment transportation and coastal fluxes. The time averaged result of D_m (Fig. 10) shows that the wave flux that, in the natural scenario, used to have a regular deflection pattern towards the coast, now has a little deflection counterclockwise near the coast. Although, in terms of direction especially, the type of comparison shown in Fig. 10 does not show a great deal of information, due to the scales involved. Thus the average of the difference of the two results was calculated and will be presented in the following section.

Finally, Fig. 11 shows the comparison of the mean values of P_w for both simulations. These results show a reduction of approximately 1.5 kW/m of wave energy potential on the position of the WEC devices. It is also noticeable a small difference of the values near the coastline. Again, since P_w is proportional to H_s squared, this result resembles the one shown in Fig. 7.

Scenario difference

To better visualize the difference caused by the wave farm and understand the possible environmental impacts of such installation, the average of the difference between the natural and the modified scenarios was calculated and will be presented hereafter.

Firstly, Fig. 12a shows the mean difference of H_s between the scenarios, showing a maximum of 0.18 m of wave height loss at the westernmost point of the wave farm. This point of maximum difference is located on that point because the mean direction of the waves is from east to west in this location (Fig. 10), thus the WEC devices on that spot will be in a “shadow” region of the other devices.

One of the perceivable effects of the D_m is the far-field effect of the converters which extends itself mostly westward.

In Fig. 12a it is easy to see the effect of the wave farm. The H_s in the coastline closest to the farm is reduced in, approximately, 8 cm. This reduction is very small compared to the order of magnitude of the H_s in this location (1.1 m), but it is worth to repeat that the distance between the WEC devices is very large, and a smaller difference could have a greater impact on the wave field.

Fig. 12b shows the increase in the T_m showed before (Fig. 8), of almost 0.3 s. This effect, contrary to H_s, does not have a large spreading beyond the wave farm. This may be related to the previous conclusion, that the difference comes from the high-frequency part of the spectrum, so once the waves leave the wave farm, the wind blows on the sea surface restoring a fraction of the lost energy.

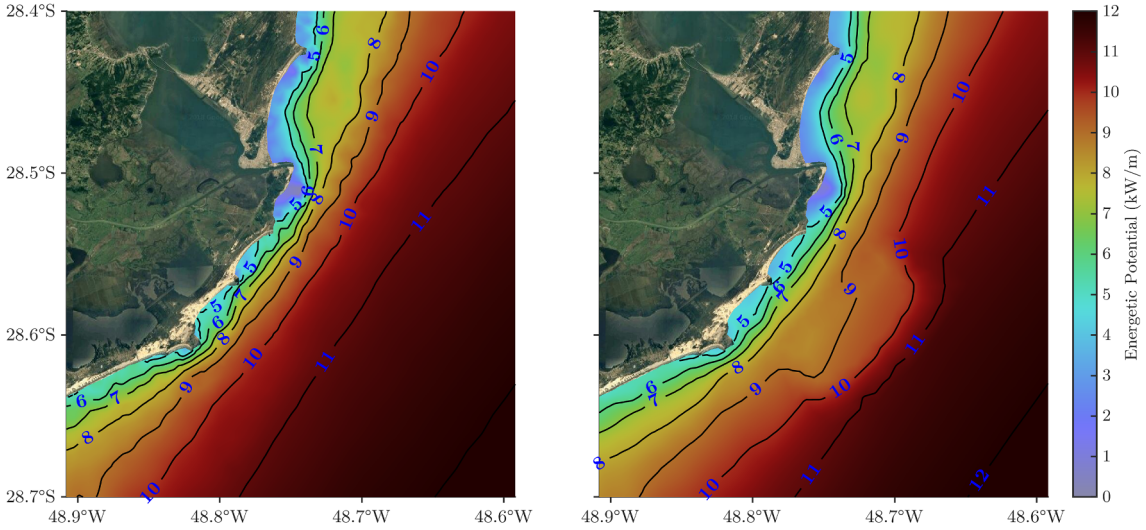

Fig. 11. Comparison of the time averaged P_w field for the (a – left) natural scenario and the (b – right) modified scenario.

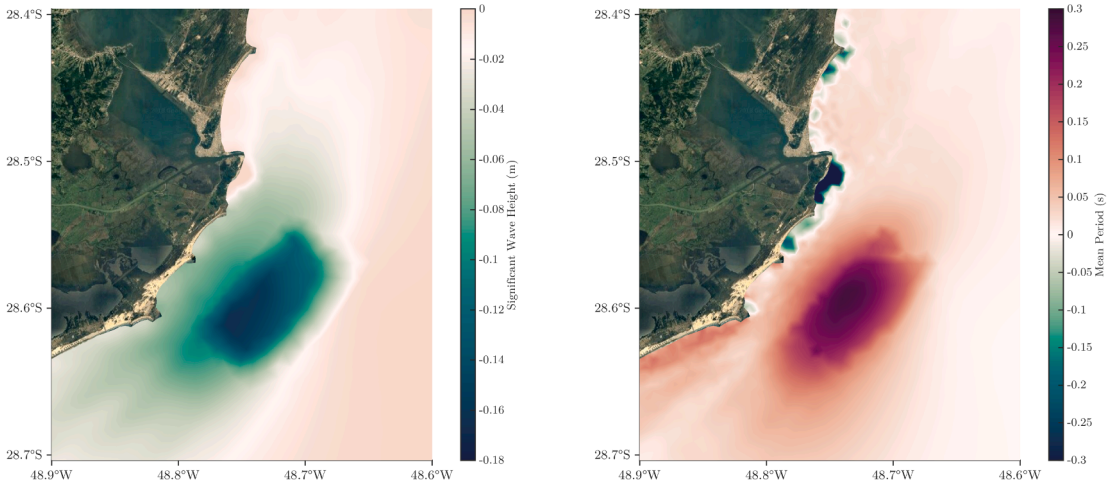

(a) Time averaged difference of H_s. (b) Time averaged difference of T_m.

Fig. 12. Time averaged difference of H_s and T_m in the study area for the year of 2014. A negative difference means that in the modified scenario there is a loss compared to the natural scenario.

The mean difference of T_p, as seen in Fig. 9 is negligible (an increase of 0.05 s) and most probably due to the numerical approximation of the peak period from the discretized spectrum. For this reason and to avoid repetition, the figure of the mean difference of T_p will be omitted.

Fig. 13a shows the mean difference of D_m on the simulated year. This figure shows the numeric value of the deflection caused by the presence of the WEC devices. Since the direction convention is positive in the clockwise direction, positive differences mean a deflection in the clockwise direction caused by the presence of the wave farm. Thus Fig. 13a shows that when entering the wave farm the waves are deflected clockwise, and when leaving it they suffer a counterclockwise deflection. This shows that the effect of the WEC devices on the wave direction is similar to a refraction effect caused by a sandbank on the sea bottom.

According to Chang et al. [38], the wave heights and associated near-bottom orbital velocities can decrease of up to 30% between baseline after the wave faces an WEC, resulting in a 15% difference in the wave height values. These authors concluded also that wave directions and periods did not appear to be sensitive to existence of a WEC device.

Finally, from Fig. 13b it is possible to see the wave energy potential lost to the converters. Once more, this figure is very similar to that of H_s (Fig. 12a), showing the greatest difference, of 1.7 kW/m, on the westernmost side of the farm. It is also possible to observe the effect of the main propagation direction of the waves in the far-field effect of the WECs, as well as the variability of the direction in the wide shadow area of the wave farm.

Additionally, Fig. 14 shows the time series of H_s extracted at every mesh node where a WEC was simulated. It can be seen that the difference is not negligible, yet it is small. The line representing the

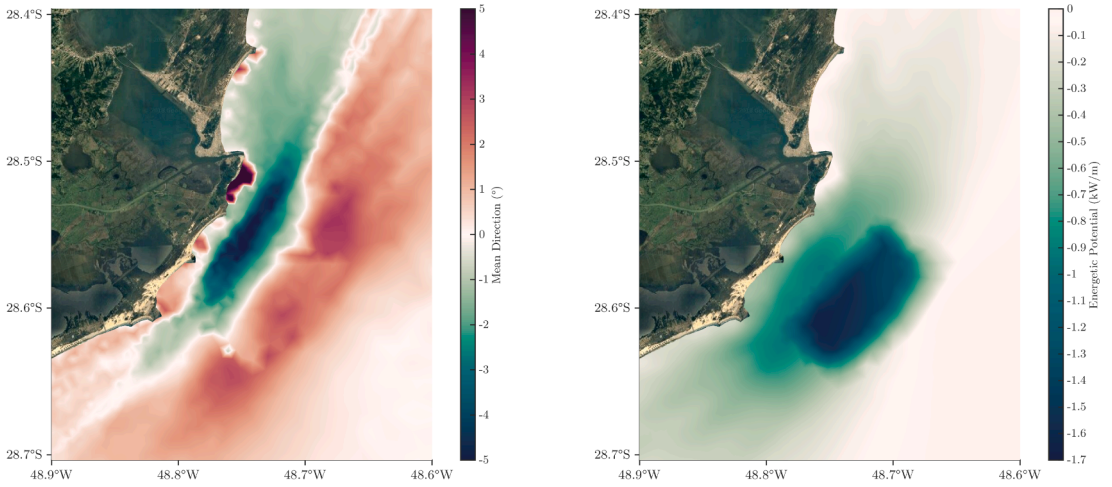

(a) Time averaged difference of D_m. (b) Time averaged difference of P_w.

Fig. 13. Time averaged difference of D_m and P_w in the study area for the year of 2014. A negative difference means that in the modified scenario there is a loss compared to the natural scenario.

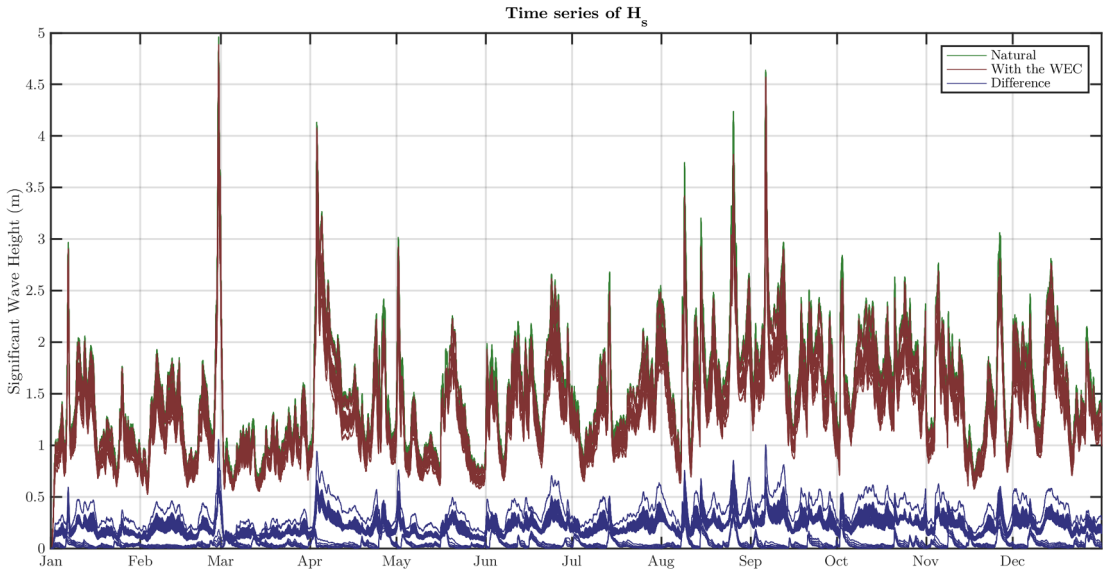

Fig. 14. Time series of H_s along the simulated year at every WEC. The natural scenario is the green lines (behind the red ones), the scenario with the WECs is the red lines, and the difference between the scenarios is represented by the blue lines.

difference is higher at some points than at others probably because the waves at the westernmost edge of the wave farm have already passed through other WECs and lost some of their energy.

From Fig. 14 one can also see that from an economical perspective, some of the WECs had little effect on the wave field, thus couldn't convert as much energy as the others did. To correct this, studies have to be made to find the best distribution of the devices in order to minimize the effect of one on another.

Conclusion

This paper featured the utilization of a novel wave energy conversion model that can be coupled with a spectral wave model to estimate the actual amount of electrical energy converted.

The mean estimated power available for conversion of the site of 131.63 kW is obtained integrating the power removed from the wave field. This value disregards any losses associated with the conversion process.

The installation of this wave farm near the coastline of Laguna – SC did not show itself as a threat to the environment because, even though the wave heights have suffered a small reduction, it was not a significant value that could bring any harm to the local hydrodynamics. Although this conclusion is being drawn solely from the analysis of the wave field, what by itself is not enough to provide concrete proof that the wave farm would or not cause future problems.

From the perspective of the wind waves, the action of the WEC devices does not change deeply the environment. The mean H_s reduction was 0.2 m, associated with an increase in 0.3 s in the mean wave period and a maximum deflection of the wave direction of 5°, in average. These values are much smaller than the changes caused by other environmental factors.

Also, these small changes in the wave field are justified by the economic benefit of the installation of the wave farm, which could reduce the cost of the energy for the cities it would supply.

In order to provide a solid argument in favor or against the installation of a wave farm, further studies should be performed considering different aspects of the project. One of them should be the utilization of different types of WEC devices and their arrangement in order to create the most economically viable configuration of the wave farm.

Another indispensable study should be the hydrodynamic analysis of the region coupled with a morphodynamic study to determine if the presence of the wave farm would not trigger erosive processes or any other drastic changes in the morphology of the region.

Once the subject is thoroughly studied, arguments could be provided to support the installation of a wave farm on this location or provide a background for the installation on other places.

Acknowledgements

The authors are grateful to the Centro de Hidrografia da Marinha (CHM) of the Brazilian Navy for the bathymetric data, the National Oceanic and Atmospheric Administration (NOAA) for the wind and wave data, and to the Open Telemac-Mascaret consortium for the continuous development of the modeling suite. This research was developed using the resources of the Centro Nacional de Supercomputação (CESUP), and the Laboratório Nacional de Computação Científica (LNCC-SDUMONT-2017-C01#166515). This study was financed in part by the Coordenação de Aperfeiçoamento de Pessoal de Nível Superior – Brasil (CAPES) – Finance Code 001, and was supported by the Fundação de Amparo à Pesquisa do Estado do Rio Grande do Sul (FAPERGS) under contracts 17/2551-001159-7, and by the Conselho Nacional de Desenvolvimento Científico e Tecnológico (CNPq) under the grant n° 304227/2016-1.

Appendix A. Supplementary data

Supplementary data associated with this article can be found, in the online version, at https://doi.org/10.1016/j.seta.2018.12.023.

References

[1] Drew B, Plummer AR, Sahinkaya MN. A review of wave energy converter technology. Proc Inst Mech Eng Part A 2009;223(8):887–902. https://doi.org/10.1243/09576509JPE782. URL:http://journals.sagepub.com/doi/10.1243/09576509JPE782, ISSN 0957-6509.

[2] Falcão AFDO. Wave energy utilization: a review of the technologies. Renew Sustain Energy Rev 2010;14(3):899–918. https://doi.org/10.1016/j.rser.2009.11.003. URL:http://linkinghub.elsevier.com/retrieve/pii/S1364032109002652. ISSN 13640321.

[3] Babarit A, Hals J, Muliawan MJ, Kurniawan A, Moan T, Krokstad J. Numerical benchmarking study of a selection of wave energy converters. Renew Energy 2012;41:44–63. https://doi.org/10.1016/j.renene.2011.10.002. URL:http://linkinghub.elsevier.com/retrieve/pii/S0960148111005672. ISSN 09601481.

[4] López I, Andreu J, Ceballos S, Martínez de Alegría I, Kortabarria I. Review of wave energy technologies and the necessary power-equipment. Renew Sustain Energy Rev 2013;27:413–34. https://doi.org/10.1016/j.rser.2013.07.009. URL:http://

linkinghub.elsevier.com/retrieve/pii/S1364032113004541. ISSN 13640321.
[5] Tiron R, Mallon F, Dias F, Reynaud EG. The challenging life of wave energy devices at sea: a few points to consider. Renew Sustain Energy Rev 2015;43:1263–72. https://doi.org/10.1016/j.rser.2014.11.105. ISSN 13640321.
[6] Day AH, Babarit A, Fontaine A, He Y-P, Kraskowski M, Murai M, et al. Hydrodynamic modelling of marine renewable energy devices: a state of the art review. Ocean Eng 2015;108:46–69. https://doi.org/10.1016/j.oceaneng.2015.05.036. URL:https://linkinghub.elsevier.com/retrieve/pii/S0029801815002280. ISSN 00298018.
[7] Amiri A, Panahi R, Radfar S. Parametric study of two-body floating-point wave absorber. J Mar Sci Appl 2016;15(1):41–9. https://doi.org/10.1007/s11804-016-1342-1. ISSN 16719433.
[8] Wang L, Isberg J, Tedeschi E. Review of control strategies for wave energy conversion systems and their validation: the wave-to-wire approach. Renew Sustain Energy Rev 2018;81:366–79. https://doi.org/10.1016/j.rser.2017.06.074. URL:http://linkinghub.elsevier.com/retrieve/pii/S136403211731016X. ISSN 13640321.
[9] Titah-Benbouzid H, Benbouzid M. An up-to-date technologies review and evaluation of wave energy converters. Int Rev Electr Eng 2015;10(1):52–61. ISSN 18276679 18276660.
[10] Ozkop E, Altas IH. Control, power and electrical components in wave energy conversion systems: a review of the technologies. Renew Sustain Energy Rev 2017;67:106–15. https://doi.org/10.1016/j.rser.2016.09.012. URL:http://linkinghub.elsevier.com/retrieve/pii/S1364032116305044. ISSN 13640321.
[11] Mustapa MA, Yaakob OB, Ahmed YM, Rheem C-K, Koh KK, Adnan FA. Wave energy device and breakwater integration: a review. Renew Sustain Energy Rev 2017;77:43–58. https://doi.org/10.1016/j.rser.2017.03.110. URL:http://linkinghub.elsevier.com/retrieve/pii/S1364032117304409. ISSN 13640321.
[12] Rusu E, Onea F. A review of the technologies for wave energy extraction. Clean Energy 2018;2(1):10–9. https://doi.org/10.1093/ce/zky003. URL:https://academic.oup.com/ce/article/2/1/10/4924611. ISSN 2515-4230.
[13] Kinsman B. Wind waves: their generation and propagation on the ocean surface. 2nd ed. New York: Dover Publications Inc; 1965.
[14] Krogstad HE, Barstow SF. Satellite wave measurements for coastal engineering applications. Coast Eng 1999;37:283–307.
[15] Mørk G, Barstow SF, Kabuth A, Pontes MT. Assessing the global wave energy potential. Proceedings of OMAE2010. Shangai: American Society of Mechanical Engineers; 2010.
[16] Gunn K, Stock-Williams C. Quantifying the global wave power resource. Renew Energy 2012;44:296–304. https://doi.org/10.1016/j.renene.2012.01.101.
[17] Reguero BG, Losada IJ, Méndez FJ. A global wave power resource and its seasonal, interannual and long-term variability. Appl Energy 2015;148:366–80. https://doi.org/10.1016/j.apenergy.2015.03.114.
[18] Oleinik PH, Marques WC, Kirinus EdP. Simulação de ondas oceânicas na costa Sul-Sudeste brasileira para análise do potencial energético. Vetor 2016;26(2):39–50. URL:https://www.seer.furg.br/vetor/article/view/6514. ISSN 2358-3452.
[19] Oleinik PH, Marques WC, Kirinus EdP. Evaluation of the seasonal pattern of wind-driven waves on the south-southeastern Brazilian shelf. Defect Diffus Forum 2017;370:141–51. https://doi.org/10.4028/www.scientific.net/DDF.370.141. ISSN 1662-9507.
[20] Oleinik PH, Marques WC, Kirinus EdP. Estimate of the wave climate on the most energetic locations of the south-southeastern Brazilian shelf. Defect Diffus Forum 2017;370:130–40. https://doi.org/10.4028/www.scientific.net/DDF.370.130. URL:http://www.scientific.net/DDF.370.130. ISSN 1662-9507.
[21] Castro BM. Summer/winter stratification variability in the central part of the South Brazil Bight. Continental Shelf Res 2014;89:15–23. https://doi.org/10.1016/j.csr.2013.12.002. URL:http://linkinghub.elsevier.com/retrieve/pii/S0278434313004081. ISSN 02784343.
[22] Dottori M, Castro BM. The response of the Sao Paulo Continental Shelf, Brazil, to synoptic winds. Ocean Dyn 2009;59(4):603–14. https://doi.org/10.1007/s10236-009-0209-2. URL:http://link.springer.com/10.1007/s10236-009-0209-2. ISSN 1616-7341.
[23] Dereczynski CP, Menezes WF. Meteorologia da Bacia de Campos. In: Martins RP, Grossman-Matheson GS, editors. Caracterização ambiental regional da Bacia de Campos, Atlântico Sudoeste: Meteorologia e Oceanografia. Habitats, vol. 2. Rio de Janeiro, Brazil: Elsevier Ltd; 2015. p. 1–54. chap. 1.
[24] Kousky VE. Pentad outgoing longwave radiation climatology for the South American sector. Rev Bras Meteorol 1988;3:217–31.
[25] da Silva M. A Frequência de fenômenos meteorológicos na América do Sul: climatologia e previsibilidade (Thesis). Universidade Federal do Rio de Janeiro; 2003.
[26] Espindola RL, Araújo AM. Wave energy resource of Brazil: an analysis from 35 years of ERA-interim reanalysis data. PLOS One.
[27] Contestabile P, Ferrante V, Vicinanza D. Wave energy resource along the coast of Santa Catarina (Brazil). Energies 2015;8(12):14219–43. https://doi.org/10.3390/en81212423. ISSN 19961073.
[28] Awk T. Tomawac User Manual Version 7.2 [Tech. Rep.]. The TELEMAC-Mascaret Consortium; 2017. 7.2.3 edition.
[29] Holthuijsen LH. Waves in oceanic and coastal waters. 1st ed. Cambridge: Cambridge University Press; 2007.
[30] Betz A. Windenergie und ihre Ausnutzung durch Windmühlen. 1st ed. Göttingen: Vandenhoeck & Ruprecht; 1926.
[31] Frigo M, Johnson SG. The design and implementation of FFTW3. Proc IEEE 2005;93(2):216–31.
[32] López-Ruiz A, Bergillos RJ, Lira-Loarca A, Ortega-Sánchez M. A methodology for the long-term simulation and uncertainty analysis of the operational lifetime performance of wave energy converter arrays. Energy 2018;153:126–35. https://doi.org/10.1016/j.energy.2018.04.018. URL:https://linkinghub.elsevier.com/retrieve/pii/S036054421830608X. ISSN 03605442.
[33] Bozzi S, Giassi M, Moreno Miquel A, Antonini A, Bizzozero F, Gruosso G, et al. Wave energy farm design in real wave climates: the Italian offshore. Energy 2017;122:378–89. https://doi.org/10.1016/j.energy.2017.01.094. URL:http://linkinghub.elsevier.com/retrieve/pii/S0360544217301019. ISSN 03605442.
[34] Guimarães RC, Oleinik PH, de Paula Kirinus E, Lopes BV, Trombetta TB, Marques WC. An overview of the Brazilian continental shelf wave energy potential. Regional Stud Mar Sci 2019;25:100446. https://doi.org/10.1016/j.rsma.2018.100446. URL:http://www.sciencedirect.com/science/article/pii/S235248551830152X. ISSN 2352-4855.
[35] Abanades J, Greaves D, Iglesias G. Coastal defence using wave farms: the role of farm-to-coast distance. Renew Energy 2015;75:572–82. https://doi.org/10.1016/j.renene.2014.10.048. URL:http://linkinghub.elsevier.com/retrieve/pii/S0960148114006752. ISSN 09601481.
[36] Iglesias G, Fernandez H, Carballo R, Castro A, Taveira-Pinto F. The WaveCat – development of a new wave energy converter. World Renewable Energy Congress, Linköping 2011. p. 2151–8. https://doi.org/10.3384/ecp110572151. URL:http://www.ep.liu.se/ecp/article.asp?issue=057%26volume=9%26article=2.
[37] Fernandez H, Iglesias G, Carballo R, Castro A, Fraguela JA, Taveira-Pinto F, Sanchez M. The new wave energy converter WaveCat: concept and laboratory tests. Mar Struct 2012;29(1):58–70. https://doi.org/10.1016/j.marstruc.2012.10.002. URL:http://linkinghub.elsevier.com/retrieve/pii/S0951833912000640. ISSN 09518339.
[38] Chang G, Ruehl K, Jones CA, Roberts J, Chartrand C. Numerical modeling of the effects of wave energy converter characteristics on nearshore wave conditions. Renew Energy 2016;89:636–48. https://doi.org/10.1016/j.renene.2015.12.048. URL:http://linkinghub.elsevier.com/retrieve/pii/S0960148115305528. ISSN 09601481.